UDC 621.865.8
DOI: 10.25140/2411-5363-2018-4(14)-66-77

Alexander Gmiterko, Ľubica Miková, Erik Prada

ANALYSIS OF AIR-SPRING FOR A LINK OF HYPER-REDUNDANT MANIPULATOR

Urgency of the research. *This research paper deals with a designing and analyzing of link for hyper-redundant manipulator/mechanism. The paper investigates 6-DOF manipulator link, consisting of pneumatic as well as electromagnetic actuators. A motion of upper platform of the link is reached by pneumatic actuators, namely air-springs. The main focus of this research is analysis of air-spring and its properties. From this reason FEM analysis is done in software SolidWorks. In the conclusion the results are discussed. Pneumatic actuators can play interesting role in order to be possible to change the mechanical properties of the manipulators.*

Target setting. *Analysis of air-spring actuator for hyper-redundant manipulator.*

Actual scientific researches and issues analysis. *Most of robotic arms consist of electrical actuators. Using pneumatic actuators the manipulator gets new properties like changing stiffness.*

Uninvestigated parts of general matters defining. *Air-springs are still in the process of investigation from the view of mechanisms actuator.*

The research objective. *In the paper simulations and analysis of the air-spring are done.*

The statement of basic materials. *This paper investigates the area of modeling in software SolidWorks. At first CAD model of new segment for hyperredundant manipulator is introduced and its basic parts are described. Then, in the preprocessing phase, the detailed steps of its setup SolidWorks computation core were described. The second half of the article is to focus on the calculation and assessment of simulation results.*

Conclusions. *The paper introduces new kind of manipulator link. The link is analyzed and tested by simulation.*

Keywords*: bellows; hyper-redundant; pneumatic joint; manipulator.*
Fig.: 12. Table: 1. References: 14.

Introduction. Nowadays, factories cannot work without manipulators and industrial robots. Using suitable kinematic structures of manipulators can be done many of required tasks in the factories like painting, cutting etc. The basic kinematic structures of manipulators like anthropomorphic, cartesian, cylindrical and polar configuration are well-known [1]. Another kind of manipulator is so-called hyper-redundant manipulator. This term was first time used by the researchers G. S. Chirikjian and J. W. Burdick in [2]. Hyper-redundant mechanism is a mechanism with many more degrees of freedom (DOF) required to perform a certain task [3]. These manipulators arise from biology for example snakes, elephant trunks, and tentacles. Implementations of hyper-redundant manipulators could be significant because of many of DOF [4]. These redundant DOF can be used for optimization tasks like obstacle avoidance task, kinematic singularity avoidance task, joint limit avoidance task etc.

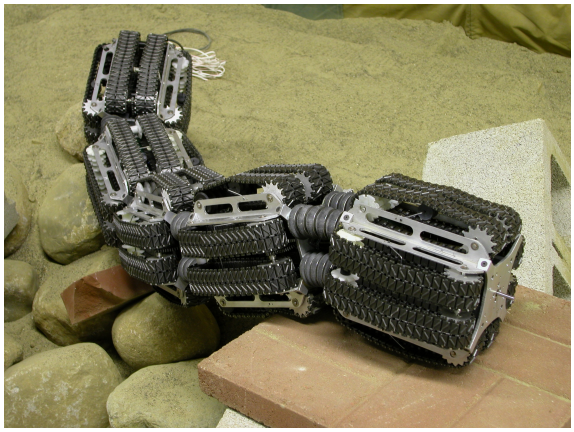

Fig. 1. OmniTread snake-like robot [6]

Our study deals with the segment of hyper-redundant manipulator of which it consists of. The work is inspired by the patent of J. Borenstein and G. Granosik [5]. Authors designed pneumatic joint, which can be used for hyper-redundant manipulator as well as snake robot, see Fig. 1. The joint consists of several air rubber bellows, universal joint and some platforms. Our contribution is design of new segment for manipulator, which consists of pneumatic as well as electromagnetic actuators.

The paper is divided into following sections: At first CAD model of new segment for hyper-redundant manipulator is introduced and its basic parts are described. Next chapter contain pre-processing phase, where detailed described steps of its setup SolidWorks computation core. The second half of the article is to focus on the calculation and assessment of simulation results.

Mechanical Design of Joint

Our aim is to design the segment for redundant or hyper-redundant manipulator which can be used for unconventional manipulation tasks. In other words, we do not want to design segment for manipulator which is usually used in factories for example in automobile industry. Our aim is rather to design manipulator for grasping tasks or tasks, concerning manipulation with the objects. Manipulator should know how to avoid to the obstacles in the environment while performing required applications. Therefore we have several requirements for possibilities of this segment, those mechanical design and its properties should be fulfilled.

Assuming that segment is developed for redundant or hyper-redundant manipulator, its structure should consists of several identical segments or segments, which can be added to the last segment in case of need. Our next requirement is 3D dexterous workspace of manipulator. The actuators of segment have to allow it to do spatial motion. Motion of segment is not bound only for one kind of actuator. Considering hyper-redundant manipulator, particular segments should be able to evolve sufficient force for manipulating with the end-effector. This point concerns primarily to segments which are near to the base of manipulator.

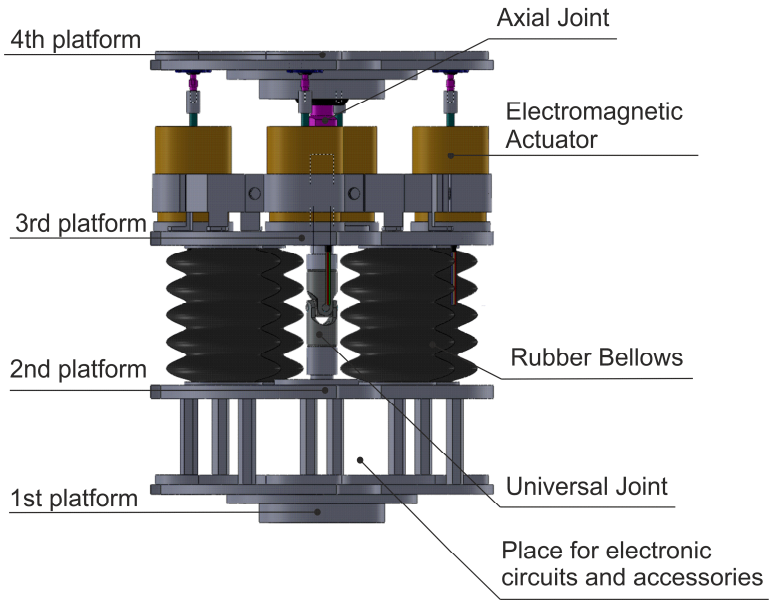

Fig. 2. Model of link for hyper-redundant manipulator

For this reason it has to be assumed there with hydraulic or pneumatic actuators which can produce significantly higher force effect in comparison with electrical actuator [6]. On the other hand, using hydraulic or pneumatic actuator we cannot reach so precise results in positioning as with using electrical actuator [7]. This reason leads us to use combination of variously kinds of actuators in one segment of manipulator.

Considering of all mentioned requirements and constraints we designed new segment for manipulator, see Fig. 2. CAD model was designed in software SolidWorks.

As can be seen in the Fig. 1, there is one universal joint enabling motion in 2 axes, located on 2nd platform. Motion is assured by four rubber bellows which are actuated by pneumatic compressor. As have been mentioned above, higher force performance can be reached by pneumatic actuator but the precision of positioning is not too sufficient. For this reason there are four electromagnetic actuators for more precise positioning used, located on the 3rd platform. These actuators have their own position sensor. On the 3rd platform also an axial joint

which allows precise positioning by means of electromagnetic actuators is located. By assuming mentioned actuators and joints the segment of hyper-redundant manipulator is 6-DOF. Material of segment construction is duraluminium and segment has weight roughly 1,4 kg.

Within our study concerning designing of the new segment of hyper-redundant manipulator we are focused on properties of rubber bellows. Extension and shortening of bellows is bounded by universal joint located on the 2nd platform.

Simulation of a pneumatic air-spring

Before the simulation itself could have been performed, we proceeded to create a virtual model in SolidWorks 2013. More specifically, it was a pneumatic bellow McKibben, the same as the one used in the case of US 6,870,343 B2 patent. The design parameters of a virtual model were consistent with a realistic model which allowed us to approximate to the truest conditions within simulation. The actual simulation consisted of verifying the behavior of a pneumatic bellow under certain pressure. It means the change of affection of individual tenseness in mechanism, the change of the size and speed. Because of this, the problem of nonlinear dynamic load was solved within simulation. In order for us to be able to simulate the possible impact of the bonds, we have defined the limits consisting of contacts on the both ends of the pneumatic mechanism. During the attempt to implement restrain rings to a simulation model, the frequent fall of the computational core occurred. We suppose that the reason for these falls was the considerable complexity of calculation during the contact of the surfaces.

The great disadvantage of the simulation of this type is a relatively time-consuming severity of the calculation itself. The increase of the required time is manifested mostly in components with intricate geometric shapes. In our case, the geometric complexity itself necessitated a minimum density of mesh required from the generator. The calculation of each simulation was conducted on a special calculating virtual machine with four shared cores (Intel Core I7) of processors with active hyperthreading. For the needs to store the operational data, the virtual computer was equipped by 8GB of memory. Important parameter for the successful implementation of the calculation in terms of the resources provided was the size of the virtual disk's capacity available. Mostly in the cases in which the calculation with a defined adaptive action of individual iterations was performed, there was a great demand for storage space. The time period of calculation of these adaptive steps have increased mostly in the cases where the possibilities of usage of hyper-elastic material properties were verified. All changes of settings and procedures relating to individual phases of simulation will therefore be introduced in separate subchapters.

In addition to the standard model of the pneumatic bellow, we tried to verify the extended model in our simulation as well. This model also included the restraint rings anchored in the individual waves of the mechanism. The function of these rings was guide the expansion pneumatic bellow. From the course of the simulations we have discovered that the usage of other structural elements within one simulation is extremely demanding for computing power as well as for the overall time that equals to tens of hours. For this reason, we carried out the simulations of the design elements separately in the final stage.

1.1 Order of steps in the phase of pre-processing and the adjustment parameters

This simulation part is very important in terms of the correct entry of the input calculation parameters. Otherwise, the bad interpretation of incorrect results could occur as the result of wrong input parameters. In the worse case, the computational core could fall. As mentioned in the previous chapter, in our case we will observe the change of behavior of the pneumatic bellow under the influence of the input pressure. Total number of pressures, which will be observed, corresponds to the number of pressure changes at experimental part of verification, see Table.

Table

Values of pressure for simulation process

Number of simulation	1.	2.	3.	4.	5.	6.	7.
Max bellow pressure (MPa)	0,006	0,042	0,065	0,113	0,142	0,192	0,238
Number of simulation	8.	9.	10.	11.	12.	13.	14.
Max bellow pressure (MPa)	0,284	0,332	0,380	0,424	0,470	0,516	0,602

At first, we have chosen a nonlinear dynamics problem to be solved and from the individual parts of simulation model, we have chosen pneumatic bellow to create a shell element. It is the solution of shell element what guarantees us more simple numerical calculation. Some reports however indicate that when dealing with pneumatic mechanisms, the non-shell element should be used, because the thickness of a shell is the same in the whole object, while non-shell element can reflect realistically the actual change of the thickness in the places of bending, see Fig. 3 [8].

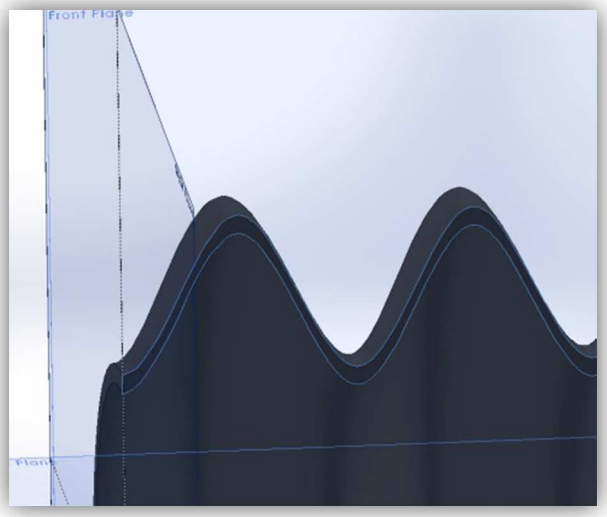

Fig. 3. Varying thickness of individual waves of the pneumatic bellow

In the second step, we have defined the material properties of simulation model. Since the simulation model consists of two different geometrical and material elements we have defined the material for every structural element separately. This definition consisted in selecting the material generated by us. More specifically, it was a type of hyper-elastic material Mooney-Rivlin, which was applied to the shell element of pneumatic mechanism. Following applies for the strain energy and the density of this type of material:

$$W = C_1\left(\overline{I}_1 - 3\right) + C_2\left(\overline{I}_2 - 3\right) \tag{1}$$

where C_1 *and* C_2 are empirical suitably chosen material constants, and $\overline{I}_1$, $\overline{I}_2$ are the first and the second invariant of unimodular Cauchy-Green components of the deformation tensor.

$$\overline{I}_1 = J^{-2/3} I_1,\ \overline{I}_2 = J^{-4/3} I_2 \tag{2}$$

$$I_1 = \lambda_1^2 + \lambda_2^2 + \lambda_3^2 \tag{3}$$

$$I_2 = \lambda_1^2\lambda_2^2 + \lambda_2^2\lambda_3^2 + \lambda_3^2\lambda_1^2 \quad (4)$$

$$J = det\left(\boldsymbol{F}\right) \quad (5)$$

F equals to deformation gradient. Due to the fact that the characteristic attribute of our material is its incompressibility, $J = 1$. Based on the works [9] the appropriate material constants were chosen: $C_1 = 1\left[\text{MPa}\right]$ a $C_2 = 0,9\ \left[\text{MPa}\right]$, while the condition $C_1 + C_2 > 0$ had to be fulfilled. In XY plane, the specific value 0,4999 have been chosen as Poisson's ratio, because of its compatibility with the settings of the computational core (for the cases of shell elements with great displacements). We have chosen the standard aluminium material as our second structural element in a simulation model.

In the next step, we have defined the conditions of the anchoring of shell element of a bellow in such a way, that it will comply with the real attachment in the structural model. Since we focused on the simulation of the pneumatic bellow itself, the anchoring was carried out at the edge of a shell element in the same way as if it was physically glued to the clip anchor. From the opposite side of the mechanism, the bond between the clip anchor and pneumatic bellow was defined. The reason for using a clip anchor in simulation was to achieve the limitation of expansion caused by the influence of pressure in the places of gluing, as well as the simulation of the certain mass, although only a symbolic one.

In this fourth step, the input values of expansion pressures have been sequentially defined. They have been changing in accordance with the values in the subsequent real experiment. Simulation behavior was examined sequentially for each initial pressure change. Since we know that a certain pressure in pneumatic bellow is achieved in nonlinear converge, for each case of pressure custom accrual curves have been defined. These have been used in setting of the pressure parameters Table 1.

The fifth step is to define Rayleigh damping coefficients. The reason why we consider this influencing factor is that we assume some damping properties of a rubber pneumatic mechanism. Since the simulation model consists of two components with different material composition and geometrical shapes, there is an assumption of mutual influence of the masses during the expansion of a mechanism. Rayleigh´s damping is defined by the following matrix entry:

$$\boldsymbol{C} = \alpha\boldsymbol{M} + \beta\boldsymbol{K}\ . \quad (6)$$

Where **C** is the damping matrix of physical, **K** is the stiffness matrix, and **M** is the mass matrix. In many cases of calculations, it is advised to neglect the coefficients α, which together with the stiffness matrix have influence in form of the friction effect of a mass. The algorithm from the work of Chowdhury and Dasgupta [10] allows us to express both α and β coefficients, whose application is important especially in cases with a high degree of vacancy of a mechanical system. The following applies for the coefficient β:

$$\beta = \frac{2\zeta_n\omega_n - 2\zeta_1\omega_1}{\omega_n^{\ 2} - \omega_1^{\ 2}} \quad (7)$$

where ω_n is the n-th natural frequency or the harmonic frequency, ω_1 is the smallest natural frequency of the structural part, ζ_n is the damping factor for the n-th natural frequency and ζ_1 is the damping factor for the lowest natural frequency. By subsequent substitution of β parameter into Equation 8 derived from Equation 6, we can express the coefficient α.

$$2\zeta_n\omega_n = \alpha + \beta\omega_n^{\ 2} \quad (8)$$

Thus obtained coefficients α and β may be installed into the program in appropriate setting. In our case, we needed to at first determine the natural frequencies of the pneumatic mechanism in order to determine these coefficients. Because of this reason, before the simula-

tion of the dynamic behavior of a pneumatic mechanism, we needed to perform frequency analysis of the pneumatic mechanism. From the results of this analysis, we obtained natural frequencies and corresponding custom shapes. The values of the damping factors were used according to the works [12].

We have defined the damping factor $\zeta_n = 0,05$ for the frequency $\omega_n = 21,602 rad.s^{-1}$ as the largest frequency of the frequency analysis. The damping factor $\zeta_n = 0,01$ was defined for the lowest frequency $\omega_1 = 3,4703 rad.s^{-1}$. After the substitution into the equations, the calculation of the coefficients was as follows:

$$\beta = \frac{2 \times 0,05 \times 21,602 - 2 \times 0,01 \times 3,4703}{21,602^2 - 3,4703^2} = 0,00460 \quad (8)$$

$$2 \times 0,05 \times 21,602 = \alpha + 0,00460 \times 21,602^2, \ \alpha = 0,01365 \quad (9)$$

We were able to substitute the resulting values of coefficients α and β into the formulas in SolidWorks environment.

In the last point of the pre-processing part, we proceeded to set the parameters of finite elements mesh. In examining the characteristics of the geometry of the pneumatic bellow we concluded that the best option is to choose the possibility of the mesh construction based on the curvilinear approach. It means that the resulting of finite elements mesh will automatically compress in places where there is a curvature of the given object. In our case it causes that generator of the mesh created a denser mesh in the areas of the mechanical waves. More specifically, the dimension of approximately MAX 3,505 [mm] was defined for the maximum size of the element. For the minimum size, the dimension of approximately MIN 1,168 [mm] was defined. Enhancement factor of individual elements was set to a value of 1,5 and the minimum number of elements in the circle was set to 8. We selected the number of integration points to 16 in the extended parameter settings of the mesh generator. These points are used to control the level of distortion of tetra hydric elements. The final shape of the model with a finite elements mesh is shown in Figure 4.

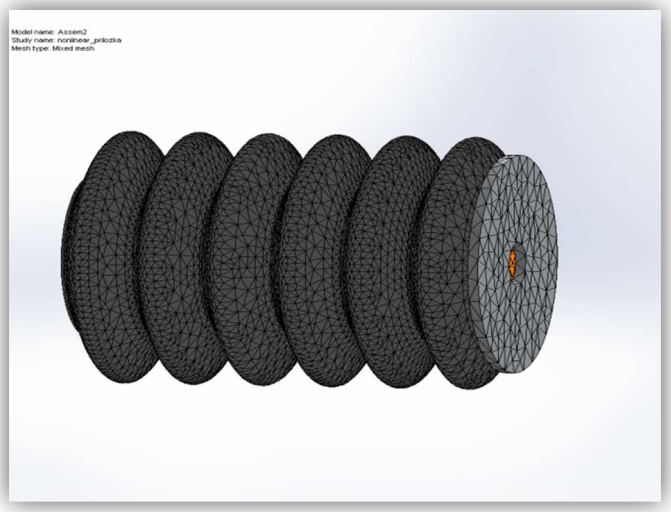

Fig. 4. Correct finite element mesh on the pneumatic bellow

1.2 Processing phase

After careful setting of all necessary parameters of pre-processing phase, we proceeded to the actual solving of the problem of non-linear dynamics of pneumatic mechanism. Before starting the SolidWorks program solver itself, we set the parameters of this solver. In Figure 5 the possible settings of the computational core are depicted.

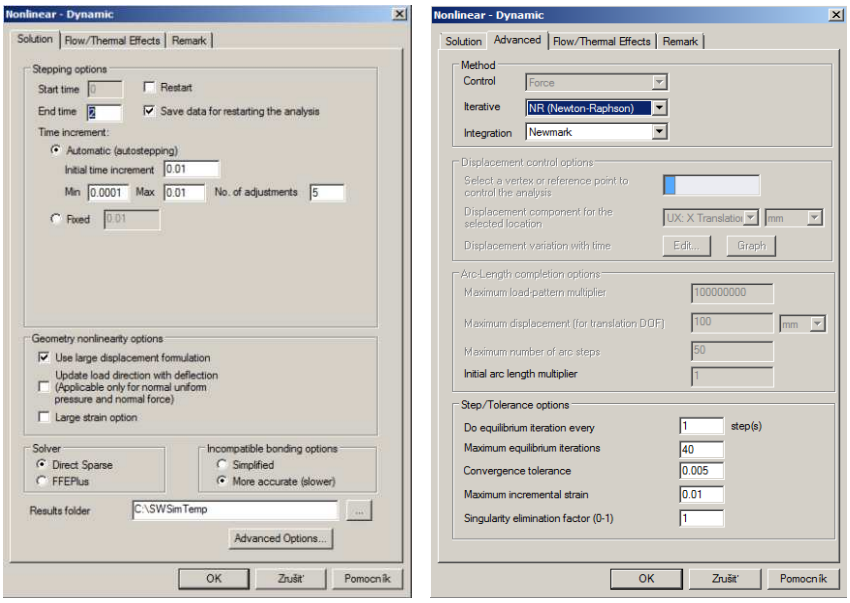

Fig. 5. Setup windows of the solver part in the SolidWorks

In "Stepping options" part, we set the finish time of the calculation to 2 seconds, which roughly corresponds to the time of experimental verification. At that time, the settling of expansion of the mechanism at a given pressure occurs. In the subsection “time increment" we have chosen the “auto stepping” of individual frames due to non-linear change of the mechanism’s shape. In the following section "Geometry nonlinearity options" we have chosen the option of large displacements, while hyper-elastic material is supposed to experience major changes of shape. It was also because of this reason, that we have chosen Direct Sparse in the section for selection of computational core "Solver". “Direct Sparse” was chosen for the direct solution of sparse matrices, which is suitable for the solution of problems with a high degree of shifts. Algorithms for the solution of sparse matrices are much more time-consuming than in the case of dense matrices, which results in the overall time complexity of this problem’s calculation. Due to the existence of contact of two structural elements of the whole simulation model, in "Incompatibile bonding options" we have chosen the option of more accurate (slower) calculation process for the case of touching areas. In the advanced settings of computation core, the Newton-Raphson method with Newmark integration has been chosen. Since in previous experiments of this calculation, the fall of computational core occurred mostly at the end of the calculation, we modified the value of maximum equilibrium iterations to 40 and reduced the value of tolerance to 0,005. After all these settings, we decided to run the calculation for each pressure change according to Table 1.

Results of the simulations of the post-processing phase

After performing the simulations, we have created graphical outputs of displacement, tenseness, deformation, velocity and acceleration according to the pressure changes listed in the chart. To illustrate the following outputs of simulations we have chosen one threshold value of pressure.

In Figure 6, the displacement of pneumatic bellow at 2 seconds since the beginning of the expansion is depicted. More specifically, we can see the maximum expansion and at the same time its displacement at the place with splice plate. Chromatic shift corresponds to the assumption that the pneumatic bellow will primarily expand in the x axis direction. The area with the lowest shift is very close to the area of anchorage of shell element. It can be concluded from the characteristic shape after the expansion that if the restraint rings were present in the calculation, the maximum length of the expansion would probably be even few millimeters greater.

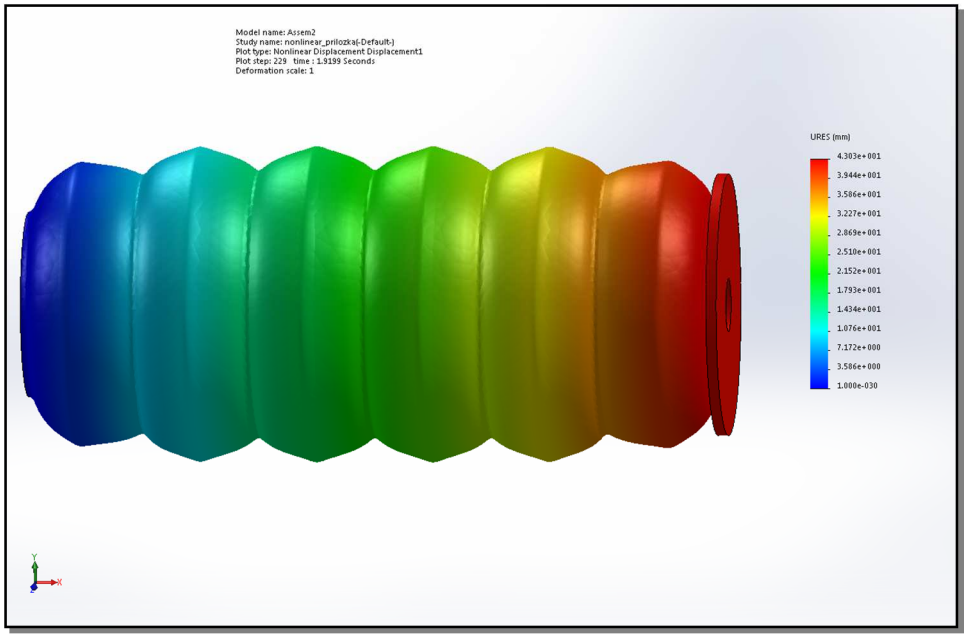

Fig. 6. Graphical representations of pneumatic bellow displacement with 0,6 [MPa] bellow pressure

Figure 7 shows the distribution of the reduced stress according to Von Mises-Hencky stress theory. The most significant effect of stress occurs in the areas of bending of the individual waves of pneumatic bellow. This means that during the expansions of the bellow, the waves expand in the direction of the x axis and at the same time, the diameter of the bellow increases. The result is the expansion of the bellow in all directions within the possibilities of the material. The depicted tenseness is the consequence of the impact of the planar tenseness in the shell.

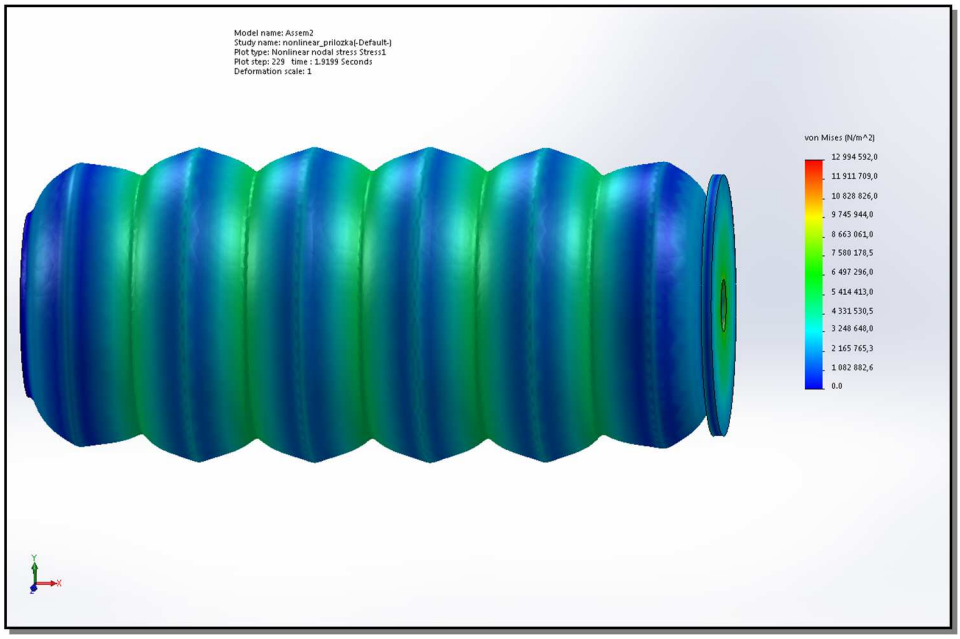

Fig. 7. Graphical representations of pneumatic bellow stress effect with 0,6 [MPa] bellow pressure

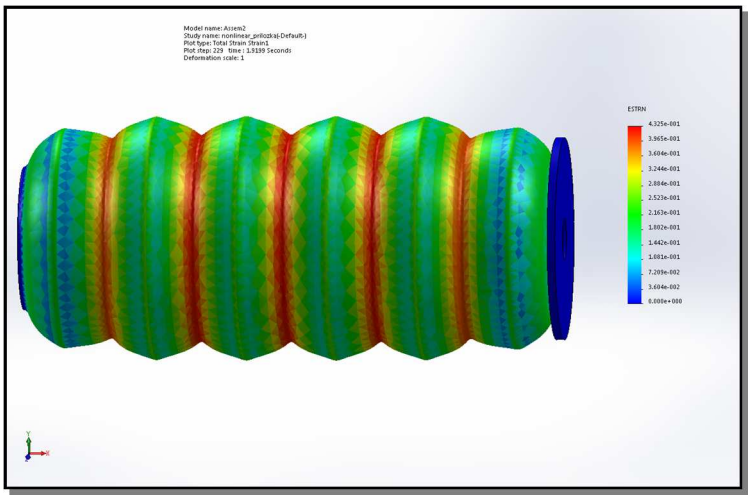

Fig. 8. Graphical representations of pneumatic bellow strain deformation with 0,6 [MPa] bellow pressure

Another important information that we have obtained from the simulation is a representation of the pneumatic bellow´s deformations in Figure 8. The greatest deformations occur in the waves that are closer to the central axis of the bellow. The reason for this is that during expansion of the bellow, the individual fibers of the material stretch along the shell element which manifests in the increase of the area. Subsequently, this area adapts to the affecting pressure in the given areas, provided that no limiting element works against the expansion. Thus, for example the deformation close to the areas of constraint and contact with the plate is smaller, since the material is trying to preserve the original geometric shape in the near surroundings. We can achieve the lowering of deformation in the areas of lower folds thanks to the restraint rings added to the structural design of restricted expansion of pneumatic bellow.

In another Figure 9 we can see the progress of velocity of individual parts of the bellow. Since the figure represents the final moment of simulation (final time interval) it is understandable that the velocities expressed are smaller compared to the velocities in the earlier time intervals. However, the character of the change of velocity along the bellow is maintained. It can be clearly seen there, that more distant parts with the splice plate have higher velocity than those which are closer to constraint.

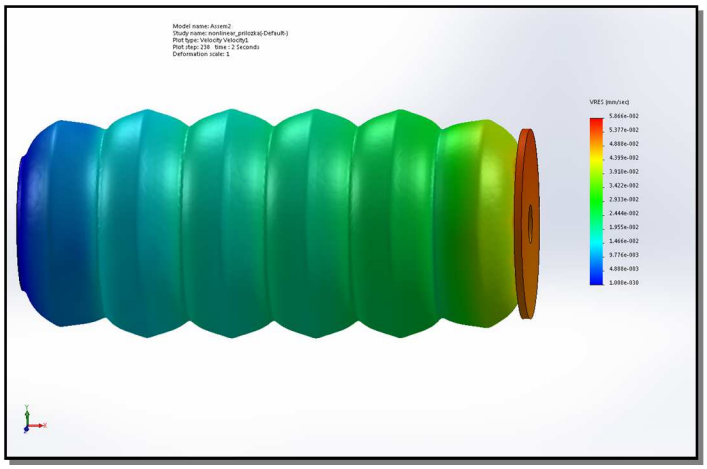

Fig. 9. Graphical representations of pneumatic bellow velocity of expansion with 0,6 [MPa] bellow pressure

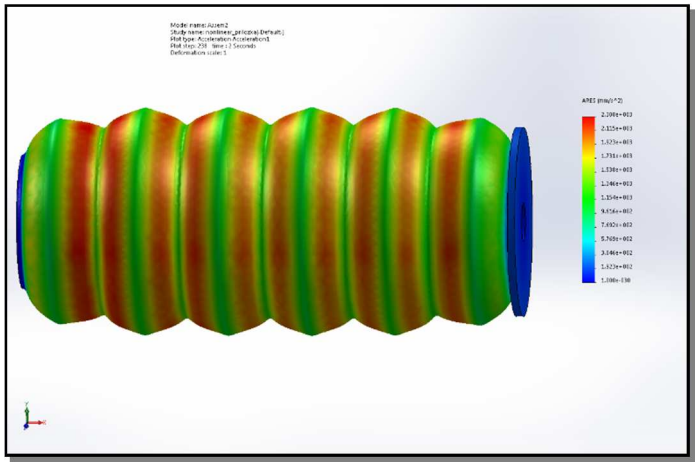

Fig. 10. Graphical representations of pneumatic bellow acceleration of expansionwith 0,6 [MPa] bellow pressure

The last variable that we were interested in during the post-processing of the simulation and its final time interval was acceleration. From Figure 10 we can conclude that the areas with the greatest acceleration are on flat surfaces which join the individual waves of the pneumatic bellow. Those areas have the greatest tenseness.

Conclusion. In conclusion, we will summarize the results of simulations at different expansion pressures and in different time intervals. In Figure 11 we can see the overall dependence of the change in increase of the shifts for individual expansion pressures of pneumatic bellow at time interval corresponding to the total simulation time. From the shape of the graph it can be seen that with the increase of pressure, the final displacement of the pneumatic bellow also increases. This increase of expansion is however, in comparison with various experimental values initially sporadic. Only at higher temperatures, the bellow begins to expand considerably. At the highest pressure values, the expansion increases, but again, sporadically. In Figure 12, the dependence of the speed of expansion of the bellow on the pressure and time of the simulation is depicted. Noticeable increases of speed are present in initial and medium simulation times, when the settling of the pressure in the bellow is expected. The character of the rising speed at increasing the final temperature is also markedly visible. It means that the air in bellow spreads faster, and as a consequence of this the expansion of pneumatic bellow is faster.

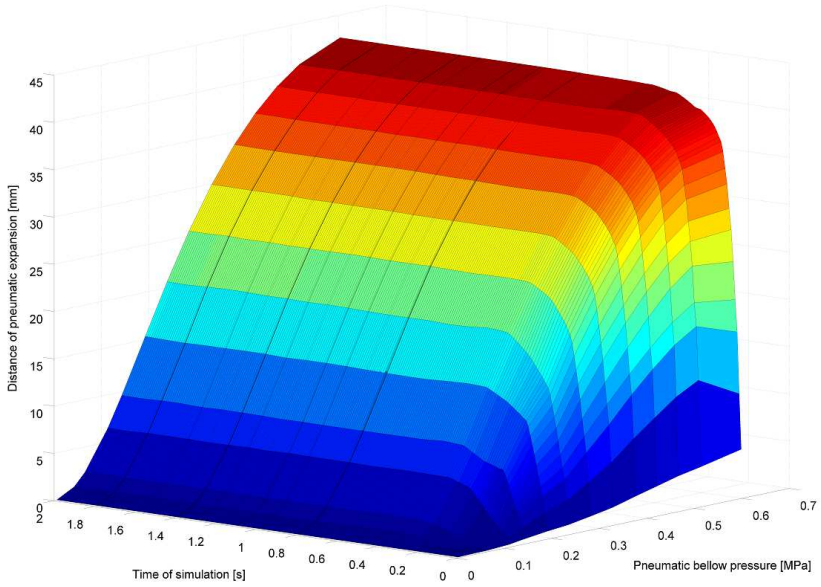

Fig. 11. The variation of displacement in the pressure change during the simulation period

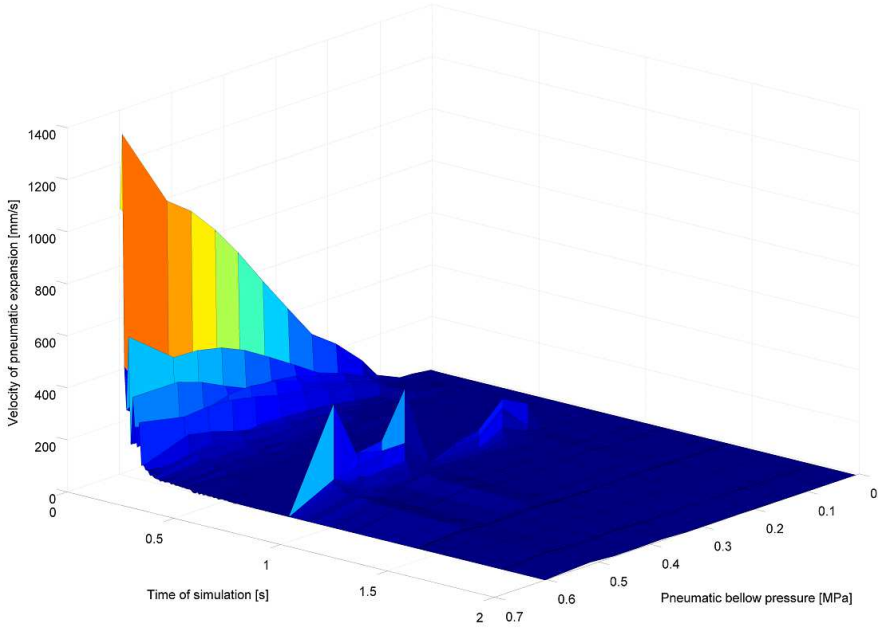

Fig. 12. The variation of velocity in the pressure change during the simulation period

Acknowledgement

This paper was supported by project VEGA1/0872/16 "Research of synthetic and biological inspired locomotion of mechatronic systems in rugged terrain" and project VEGA 1/0389/18 "Research on kinematically redundant mechanisms".

References

1. *D. Koniar*, L. Hargaš, M. Hrianka, V. Bobek, P. Drgoňa, P. Fibich, Kinematics analysis of biomechanical systems using image analysis, Metalurgija (Metallurgy), Vol. 49 (2/2010), ISSN 1334-2576.

2. *G. S. Chirikjian*, J. W. Burdick, An Obstacle Avoidance Algorithm for Hyper-Redundant Manipulators, IEEE Transaction on Robotics and Automation (1990), pp. 625 – 631.

3. *H. B. Brown*, M. Schwerin, E. Shammas, H. Choset, Design and Control of a Second-Generation Hyper-Redundant Mechanism, IEEE International Conference on Intelligent Robots and Systems (2007), pp. 2603 – 2608.

4. *G. S. Chirikjian*, J. W. Burdick, Parallel Formulation of the Inverse Kinematics of Modular Hyper-Redundant Manipulators, IEEE International Conference on Robotics and Automation (1991), 708–713.

5. *J. Borenstein*, G. Granosik, Integrated, Proportionally Controlled, and Naturally Compliant Universal Joint Actuator with Controllable Stifness, United States Patent (2005).

6. *G. Granosik*, J. Borenstein, Integrated Joint Actuator for Serpentine Robots, IEEE/ASME Transaction on Mechatronics (2005), Vol. 10, No 5, pp. 473 – 481.

7. *R. Harťanský*, V. Smieško, L. Maršálka, Numerical Analysis of Isotropy Electromagnetic Sensor Measurement Error, Measurement Science Review, Vol. 13, No. 6, pp. 311-314, ISSN 335-8871.

8. *D. Samek*, J. Javorik. Numerical Analysis of Shape Stability of Rubber Boot, International Journal of Mechanics, Vol. 7, No. 3, pp. 294-301, ISSN: 1998-4448.

9. *Oliver A.* Shergold, Norman A. Fleck, D. Radford. The uniaxial stress versus strain response of pig skin and silicone rubber at low and high strain rates, International Journal of Impact Engineering (2006), Vol. 32, pp. 1384-1402, ISSN: 0734-743X.

10. *I. Chowdhury*, S. Dasgupta. Computation of Rayleigh Damping Coefficients for Large System, The Electronic Journal of Geotechnical Engineering (2003), Vol. 8, Bundle 8C.

11. *Wiliam W. Feng*, John O. Hallquist. On Mooney-Rivlin Constants for Elastomers, 12. th. International LS-DYNA Users Conference, pp. 1-10.

12. *Detailed* vibration isolation theory. Farrat isolevel Ltd. (2014) online: http://www.farrat.com

13. *Richad Q. van der Linde*. Design, Analysis, and Control of a Low Power Joint for Walking Robots, by Phasic Activation of McKibben Muscles, IEEE Transactions on Robotics and Automation (1999), Vol. 15, No. 4, pp. 599-604, ISSN: 1042-296X.

14. *Ruiyi Tang*, Dikai Liu. An Enhanced Dynamic Model for McKibben Pneumatic Muscle Actuators, Proceedings of Australasian Conference on Robotics and Automation (2012), Victoria University of Wellington, New Zealand.

УДК 621.865.8

Олександр Гмитерко, Любіца Мікова, Ерік Прада

АНАЛІЗ ПНЕВМАТИЧНОЇ ПРУЖИНИ З'ЄДНАННЯ ГІПЕРНАДЛИШКОВОГО МАНІПУЛЯТОРА

Актуальність теми дослідження. *Ця дослідницька робота присвячена розробці та аналізу з'єднання гіпернадлишкового маніпулятора/механізму. У статті досліджується ланка маніпулятора 6-DOF, що складається з пневматичних і електромагнітних приводів. Переміщення верхньої платформи з'єднання досягається пневматичними приводами, а саме пневматичними пружинами. Основним напрямком цього дослідження є аналіз пневматичної пружини та її властивостей. З цієї причини аналіз FEM виконується в програмному забезпеченні SolidWorks. У висновку обговорюються результати. Пневматичні приводи можуть відігравати цікаву роль, як можливість змінювати механічні властивості маніпуляторів.*

Постановка проблеми. *Аналіз пнемо-пружного приводу для гіпернадлишкового маніпулятора.*

Аналіз останніх досліджень і публікацій. *Більшість маніпуляторів складається з електричних приводів. Використання пневматичних приводів надає маніпуляторам нових властивостей, таких як зміна жорсткості.*

Виділення недосліджених частин загальної проблеми. *Пневматичні пружини все ще знаходяться в процесі дослідження з точки зору механізмів приводу.*

Постановка завдання. *У статті проведено моделювання та аналіз пневматичної пружини.*

Виклад основного матеріалу. *У цій статті досліджено сферу моделювання в програмному забезпеченні SolidWorks. Спершу побудована CAD модель нового сегмента для гіпернадлишкового маніпулятора і описані його основні частини. Далі на етапі попередньої обробки детально описані кроки та налаштування для обчислювального ядра SolidWorks. Друга половина статті зосереджена на розрахунках та оцінці результатів моделювання.*

Висновки відповідно до статті. *У статті представлено новий вид з'єднання маніпулятора. З'єднання аналізується і тестується за допомогою моделювання.*

Ключові слова: *сільфонний; гіперрезервірованний; пневматичний; маніпулятор.*

Рис.: 12. Табл.: 1. Бібл.: 14.

Alexsander Gmiterko – professor, Technical University of Košice, Faculty of Mechanical Engineering, Institute of Automation, Mechatronics and Robotics, Department of Mechatronics (Letná 9, 042 00 Košice).

Ľubica Miková – assistant professor, Technical University of Košice, Faculty of Mechanical Engineering, Institute of Automation, Mechatronics and Robotics, Department of Mechatronics (Letná 9, 042 00 Košice).

Erik Prada – researcher, ZTS VVU Košice, a.s., Južná trieda 95, 041 24 Košice.

Gmiterko, A., Miková, Ľ., Prada, E. (2018). Analysis of air-spring for a link of hyper-redundant manipulator. *Technical sciences and technologies, 4* (14), 66-77.